Published in final edited form as:
Structure. 2010 December 8; 18(12): 1617–1631. doi:10.1016/j.str.2010.09.012.

Structural basis for the differential effects of CaBP1 and calmodulin on $Ca_V1.2$ calcium-dependent inactivation

Felix Findeisen[1,3] and **Daniel L. Minor Jr.**[1,2,3,4,*]

[1]Cardiovascular Research Institute, University of California, San Francisco, California 94158-2330

[2]Departments of Biochemistry and Biophysics, and Cellular and Molecular Pharmacology, University of California, San Francisco, California 94158-2330

[3]California Institute for Quantitative Biomedical Research, University of California, San Francisco, California 94158-2330

[4]Physical Biosciences Science Division, Lawrence Berkeley National Laboratory, Berkeley, CA 94720 USA

Abstract

Calcium-binding protein 1 (CaBP1), a calmodulin (CaM) homolog, endows certain voltage-gated calcium channels (Ca_Vs) with unusual properties. CaBP1 inhibits $Ca_V1.2$ calcium-dependent inactivation (CDI) and introduces calcium-dependent facilitation (CDF). Here, we show that the ability of CaBP1 to inhibit $Ca_V1.2$ CDI and induce CDF arises from interaction between the CaBP1 N-lobe and interlobe linker residue Glu94. Unlike CaM, where functional EF hands are essential for channel modulation, CDI inhibition does not require functional CaBP1 EF-hands. Furthermore, CaBP1-mediated CDF has different molecular requirements than CaM-mediated CDF. Overall, the data show that CaBP1 comprises two structural modules having separate functions: similar to CaM, the CaBP1 C-lobe serves as a high-affinity anchor that binds the $Ca_V1.2$ IQ domain at a site that overlaps with the Ca^{2+}/CaM C-lobe site, whereas the N-lobe/linker module houses the elements required for channel modulation. Discovery of this division provides the framework for understanding how CaBP1 regulates Ca_Vs.

Introduction

Voltage-gated calcium channels (Ca_Vs) serve as a major source of calcium influx in excitable cells (Catterall, 2000). Because calcium ions are chemical messengers (Clapham, 2007), influx through Ca_Vs can directly link membrane potential charges to stimulation of intracellular signaling cascades (Catterall, 2000). Although high-voltage activated Ca_Vs consist of four essential components (Van Petegem and Minor, 2006): a Ca_V1 or Ca_V2 pore-forming $Ca_V\alpha_1$ (Catterall, 2000), a cytoplasmic $Ca_V\beta$ (Dolphin, 2003), $Ca_V\alpha_2\delta$ (Davies et al., 2007), and calmodulin (CaM) (Pitt, 2007), the composition of these large protein complexes is not monolithic. In some contexts, such as cerebellar and hippocampal neurons (Lee et al., 2002; Zhou et al., 2004), photoreceptor synapses (Haeseleer et al., 2004), and

*Correspondence: daniel.minor@ucsf.edu .

auditory hair cells (Cui et al., 2007; Yang et al., 2006), members from a family of calcium binding proteins homologous to CaM, known as CaBPs (Haeseleer et al., 2000), can replace CaM. This component exchange has profound effects on how Ca_Vs respond to calcium entry and results in channels that have strikingly different functional properties than those modulated by CaM (Cui et al., 2007; Few et al., 2005; Lautermilch et al., 2005; Lee et al., 2002; Yang et al., 2006; Zhou et al., 2004; Zhou et al., 2005).

When modulated by CaM, many Ca_V1s exhibit a strong calcium-dependent inactivation (CDI) that limits calcium influx during depolarization (Dunlap, 2007). In contrast, Ca_V1s under the influence of CaBP1, a CaBP abundant in the brain and retina (Haeseleer et al., 2000), have dramatically altered functional properties. CaBP1 blocks $Ca_V1.2$ (Zhou et al., 2004; Zhou et al., 2005) and $Ca_V1.3$ (Cui et al., 2007; Yang et al., 2006) CDI and introduces an increase in $Ca_V1.2$ (Zhou et al., 2004) peak current upon repetitive stimulation, calcium-dependent facilitation (CDF). These effects depend on displacement of CaM from the $Ca_V\alpha_1$ C-terminal IQ domain (Yang et al., 2006; Zhou et al., 2004), a channel element that is critical for CaM-mediated CDI (Erickson et al., 2003; Zühlke et al., 1999).

As with many calcium sensor proteins (Burgoyne et al., 2004; Haeseleer et al., 2002; Weiss and Burgoyne, 2002), both CaBP1 and CaM comprise two lobes that bear a pair of EF-hand calcium binding motifs (Haeseleer et al., 2000). Beyond this common architecture, there are a number of differences. CaBP1 is myristoylated at its N-terminus, has an N-lobe that is largely insensitive to calcium (K_d > 100 μM) (Wingard et al., 2005), and a longer interlobe linker. Apart from recent NMR structures of individual CaBP1 lobes (Li et al., 2009), little is known about the high-resolution structure of complete CaBPs or the details of how they interact with Ca_Vs. Thus, it has remained uncertain which CaBP1 features contribute to the stark functional differences that CaBP1 brings to Ca_V modulation.

We set out to answer this question with respect to $Ca_V1.2$ and find that the key element is an interaction between the N-lobe and an interlobe linker residue that is conserved among CaBP family members. We further show that CaBP1 comprises two structural modules having separate functions. The CaBP1 C-lobe shares both structural and functional similarity with the CaM C-lobe and acts as a high-affinity anchor that binds the $Ca_V1.2$ IQ domain at a site that overlaps with the Ca^{2+}/CaM C-lobe binding site. In contrast, the N-lobe/linker module contains the elements required for the unique functional effects CaBP1 has on $Ca_V1.2$. Delineation of these conserved CaBP structural elements provides the required framework for understanding how this family of calcium sensor proteins affects Ca_Vs and other target proteins in a manner distinct from CaM.

Results

CaBP1 N-lobe and interlobe linker are crucial for CDI inhibition

We used two-electrode voltage clamp recording of *Xenopus* oocytes to test whether CaBP1 N-terminal myristoylation contributes to CaBP1 modulation of $Ca_V1.2$ as this lipid anchor is important for CaBP1 modulation of $Ca_V2.1$ (Few et al., 2005) and is an obvious difference from CaM (Figure 1A). Examination of calcium currents produced when $Ca_V1.2$ was co-expressed with a CaBP1 G2A mutant (Few et al., 2005) that blocks myristoylation (Rocque et al., 1993) demonstrated that CaBP1 G2A could inhibit CDI as effectively as wild type CaBP1 (Figures 1B and C, and Table 1). The enzyme that carries out myristoylation is unable to process G2A substrates and is conserved (Rocque et al., 1993). Nevertheless, to ensure that the N-terminal modification was eliminated, we also examined the consequences of deletion of the entire CaBP1 myristoylation site, CaBP1(Δ2-15). Similar to CaBP1 G2A, CaBP1(Δ2-15) fully inhibited CDI (Figures 1B and C, and Table 1). Thus, N-terminal myristoylation is not required for CaBP1 inhibition of $Ca_V1.2$ CDI.

Because CaBP1 (Li et al., 2009) and CaM (Masino et al., 2000; Tsalkova and Privalov, 1985) lobes fold independently, we designed a set of CaBP1-CaM chimeras based on exchange of three elements (N-lobe, interlobe linker, and C-lobe) and tested their effects on $Ca_V1.2$ expressed in *Xenopus* oocytes. We designate the chimeras with three letter names, *e.g.* MMB, in which the first, second, and third positions denote N-lobe, interlobe linker, and C-lobe, respectively, and each letter denotes the element origin: 'M' for CaM and 'B' for CaBP1.

All CaM N-lobe chimeras (MMB, MBB, MBM) lacked the hallmark $Ca_V1.2$ CDI inhibition caused by CaBP1, and instead supported CDI similar to CaM (Figures 1D, E, and Table 1). CaM interlobe linker chimeras (MMB, BMB and BMM) also allowed CDI to proceed. Notably, the chimera having the CaM interlobe linker exchanged into CaBP1, BMB, failed to inhibit CDI. Pulldown assays showed that all chimeras retained ability to interact with the $Ca_V1.2$ IQ domain (Figure S1) and eliminate the possibility that the absence of CDI inhibition arose from failure of the chimeras to fold properly and bind the $Ca_V1.2$ IQ domain. Together, these results suggest that the inability of MMB, MBB, MBM, MMB, BMB, and BMM to inhibit CDI arises from the absence of elements in the CaBP1 N-lobe (MMB, MBB, MBM, MMB) and CaBP1 interlobe linker (MMB, BMB, and BMM). In further support of this, we found that BBM, which has CaBP1 N-lobe and interlobe linker joined to CaM C-lobe, blocks $Ca_V1.2$ CDI even more potently than CaBP1 (Figures 1D and E). BBM additionally causes slower $Ca_V1.2$ activation (Figure 1E). Taken together, the results from the chimeras strongly suggest that the key elements underlying the CaBP1 and CaM functional differences with respect to CDI reside in the N-terminal lobe and interlobe linker.

Besides CDI inhibition, CaBP1 causes $Ca_V1.2$ CDF (Zhou et al., 2004) (Figure 1F). We tested whether the CaBP1-CaM chimeras retained this property. Chimeras bearing either the CaM N-lobe (MMB, MBB, MBM, MMB) or CaM interlobe linker (MMB, BMB, and BMM) were unable to support $Ca_V1.2$ CDF. Except for BMB, which introduced a larger progressive loss in current amplitude (Figures 1F and G), channels expressed with these chimeras were indistinguishable from channels expressed with CaM. In contrast, BBM caused $Ca_V1.2$ CDF that was ~2-fold stronger than that of CaBP1 (Figures 1F and G). Hence, BBM embodies both main functional properties of CaBP1, the ability to inhibit $Ca_V1.2$ CDI and the ability to confer CDF. Together, the data indicate that the CaBP1 N-lobe and interlobe linker bear the modulatory elements unique to CaBP1, whereas CaBP1 and CaM C-terminal lobes perform similar functions.

CaBP1 interlobe linker functional properties

The CaBP1 and CaM interlobe linker lengths differ by four residues (Figure 1A), a divergence conserved among CaBPs (Haeseleer et al., 2000) (Figure S2). Given the apparent importance of the interlobe linker, we investigated whether its length, composition, or both were crucial for CaBP1 function. CaBP1 constructs having an interlobe linker composed of the first four (93-96, 'AETA') or last four interlobe linker residues (97-100, 'DMIG') failed to inhibit CDI (Figures 2A and B). Replacement of the CaBP1 interlobe linker with a duplication of the CaM interlobe linker (DTDSDTDS), octa-alanine (8A), or octa-glycine (8G) also failed to inhibit CDI (Figures 2A and B).

Unexpectedly, the protocol used to induce CDF caused $Ca_V1.2$ to display a strong, calcium-dependent reduction in current amplitude in the presence of all of the CaBP1 interlobe linker mutants (Figure 2C). This phenomenon, which we term 'CDI tachyphylaxis', is stronger than the small current suppression seen with CaM (Figure 2D) and provides evidence that the interlobe linker manipulations did not incapacitate the CaBP1 mutants. This is corroborated by pulldown experiments that show the individual mutants retain the ability to

bind the $Ca_V1.2$ IQ domain (Figure S1B). Further analysis of the DMIG mutant showed that the CDI tachyphylaxis arises from changes in recovery from inactivation (Figures 2E). Following a depolarization pulse, $Ca_V1.2$ co-expressed with CaM shows essentially full recovery after 750 ms. In contrast, ~7% of $Ca_V1.2$ co-expressed with DMIG fail to recover in the same period. Over longer interpulse periods, both CaM and DMIG containing channels recover fully (Figure 2E). Taken together, the data from the chimeras and interlobe linker mutants establish that both the length and composition CaBP1 interlobe linker are crucial for modulation of $Ca_V1.2$.

N- and C-lobes contribute to CaBP1-$Ca_V1.2$ IQ domain affinity

We turned to isothermal titration calorimetry (ITC) to investigate how CaBP1 interacts with the $Ca_V1.2$ IQ domain, the domain that is essential for CaBP1 CDI inhibition (Zhou et al., 2004). Experiments using individual CaBP1 lobes in the presence of 1 mM calcium, Ca^{2+}/N-$lobe_{BP}$ and Ca^{2+}/C-$lobe_{BP}$, revealed that each has a single binding site on the $Ca_V1.2$ IQ domain (Figure 3A, B and Table 2). Ca^{2+}/N-$lobe_{BP}$ binding is an endothermic reaction having modest affinity (K_d = 1.11 ± 0.08 μM), whereas Ca^{2+}/C-$lobe_{BP}$ binds ~100-fold stronger via an exothermic reaction that has an affinity (K_d = 10.5 ± 1.9 nM) similar to Ca^{2+}/C-$lobe_{CaM}$ (Van Petegem et al., 2005). Competition experiments in which Ca^{2+}/N-$lobe_{BP}$ was titrated into a pre-formed Ca^{2+}/C-$lobe_{BP}$-$Ca_V1.2$ IQ domain complex demonstrate that Ca^{2+}/C-$lobe_{BP}$ prevents Ca^{2+}/N-$lobe_{BP}$ binding and indicate that the binding sites overlap (Figure 3C). As expected from the affinity differences, Ca^{2+}/C-$lobe_{BP}$ can displace Ca^{2+}/N-$lobe_{BP}$ from the $Ca_V1.2$ IQ domain (Figure 3D). The ability of both Ca^{2+}/CaBP1 lobes to bind the $Ca_V1.2$ IQ domain at an overlapping site is reminiscent of the behavior of individual Ca^{2+}/CaM lobes (Kim et al., 2008; Van Petegem et al., 2005).

Unlike the simple, individual lobe binding isotherms, titration of full-length Ca^{2+}/CaBP1 into the $Ca_V1.2$ IQ domain showed a V-shaped isotherm that could not be attributed to a single binding event (Figure 3E). Because Ca^{2+}/N-$lobe_{BP}$ and Ca^{2+}/C-$lobe_{BP}$ bind to the $Ca_V1.2$ IQ domain in a competitive manner, we wondered whether the complex isotherm arose from contributions of each lobe. ITC experiments in which equimolar portions of individual Ca^{2+}/CaBP1 lobes were titrated into the $Ca_V1.2$ IQ domain produced a binding isotherm very similar to that of full-length Ca^{2+}/CaBP1 (Figure 3F). Further, when we used parameters from the single lobe experiments to simulate the isotherm in which Ca^{2+}/N-$lobe_{BP}$ and Ca^{2+}/C-$lobe_{BP}$ bind to a single, overlapping IQ domain site, we found excellent correspondence to the measured isotherm (Figure 3F, red triangles). These results indicate that the ‘V’-shaped nature of the isotherm represents a sequence of two events: (1) independent binding of Ca^{2+}/N-$lobe_{BP}$ and Ca^{2+}/C-$lobe_{BP}$ to separate $Ca_V1.2$ IQ domains when the IQ domain is in excess, and (2) replacement of Ca^{2+}/N-$lobe_{BP}$ by Ca^{2+}/C-$lobe_{BP}$ as the IQ domain becomes limiting. The ability to dissect the binding reaction this way set the stage for an experiment to determine the thermodynamics of the Ca^{2+}/CaBP1- $Ca_V1.2$ IQ domain interaction and test whether the ‘V’-shaped isotherm observed with full-length Ca^{2+}/CaBP1 (Figure 3E) arose from a similar course of events.

Titration of Ca^{2+}/CaBP1 into pre-formed Ca^{2+}/N-$lobe_{BP}$-$Ca_V1.2$ IQ domain complexes yielded a titration isotherm having a single transition (Figure 3G). Analysis using competition ligand binding by displacement (Sigurskjold, 2000) in the context of the Figure 3H thermodynamic cycle reveals that Ca^{2+}/CaBP1 binds the $Ca_V1.2$ IQ domain ~40-fold stronger than measured for Ca^{2+}/C-$lobe_{BP}$ alone (K_d= 296 ± 70 pM)(Table 2). This increased affinity is accompanied by a binding enthalpy increase that indicates that Ca^{2+}/N-$lobe_{BP}$, the interlobe linker, or both contribute to the binding reaction by interacting with the $Ca_V1.2$ IQ domain at sites separate from the Ca^{2+}/C-$lobe_{BP}$ binding site. Taken together, the ITC experiments establish that CaBP Ca^{2+}/C-lobe interacts with the $Ca_V1.2$ IQ domain in a

manner similar to Ca^{2+}/CaM C-lobe, and show that elements from the entire CaBP1 participate $Ca_V1.2$ IQ domain binding.

Functional EF-hands not required for CDI inhibition

CaBP1 has four EF hands; however, the importance of metal binding to N-lobe EF-hands is unclear. EF1 has weak Ca^{2+} affinity (Wingard et al., 2005) and EF2 is non-functional due to the lack of a canonical residue at the 'z' position (Figure 1A)(Gifford et al., 2007; Haeseleer et al., 2000). To test whether CaBP1 inhibition of $Ca_V1.2$ CDI requires the ability of the CaBP1 EF-hands to bind metal ions, we examined the consequences of introduction of a D→A mutation at the 'x' position of each functional EF hand. This mutation is analogous to those used to dissect CaM EF hand function (Peterson et al., 1999) and should reduce metal-binding ability substantially and. CaBP1 bearing a disrupted EF1 was functionally indistinguishable from wild-type (Figures 4A and B, and Table 1). In contrast, EF3, EF4, and EF34 mutations diminished but did not eliminate the ability of CaBP1 to inhibit $Ca_V1.2$ CDI. Thus, the capacity of CaBP1 C-lobe EF hands to bind metal ions is important but not essential for CDI inhibition. This relative insensitivity to EF hand disruption stands in contrast to CaM where functional C-lobe EF-hands are required for CDI (Alseikhan et al., 2002; Peterson et al., 1999). The effects of CaBP1 EF34 are reminiscent of the ability of the CaM EF34 mutant to block CDI (Peterson et al., 1999) and suggest that part of the CaBP1 mechanism may be competition with apo-CaM. In contrast to the minor effects on CDI inhibition, the EF3 and EF4 mutants greatly diminished $Ca_V1.2$ CDF (Figure 4C and D) and indicate that CaBP1-mediated CDF requires Ca^{2+} binding to the C-lobe.

CaBP1 crystal structure

To understand how the CaBP1 N-lobe and interlobe linker contribute to function, we crystallized and determined the structure of the CaBP1 functional core, CaBP1(Δ2-15). CaBP1(Δ2-15) crystallized in the I23 space group and diffracted X-rays to 2.9Å (Table 3). Surface entropy reduction (Derewenda and Vekilov, 2006) identified a mutant, CaBP1(Δ2-15) K130A, that did not alter function (Table 1), gave crystals having a different space group, $P3_121$ and improved resolution, 2.4Å, and that enabled solution by MAD (Hendrickson and Ogata, 1997) using selenomethionine-substituted protein. The 2.4Å structure was used for molecular replacement of the I23 crystal form. As there were no major differences between the structures, we used chain A from the 2.4Å structure for analysis.

CaBP1 has four EF-hands arranged into two lobes. Unexpectedly, a well-ordered interlobe linker (residues 93-100) connects the lobes (Figure 5A). N-lobe EF hands, EF1 and EF2, lack ligands; whereas C-lobe EF hands, EF3 and EF4, each contain a calcium ion. The compact structure is different from what has been observed by NMR, which found independent lobes and a disordered interlobe linker (Li et al., 2009). Comparison with crystal structures of compact (Fallon and Quiocho, 2003) and extended (Wilson and Brunger, 2000) Ca^{2+}/CaM conformations reveals that the CaBP1 lobe orientation is different from both (Figure S3A). Despite the compact conformation, the CaBP1 lobes make few contacts with each other and bury only 270 $Å^2$.

N-lobe is in the calcium-free apo-form. Neither EF1 nor EF2 have electron density indicative of a metal ion, despite crystallization conditions containing millimolar Ca^{2+}. Apo-N-lobe shows a number of differences from the Mg^{2+}-bound N-lobe NMR structure (Li et al., 2009) ($RMSD_{C\alpha}$=2.5Å). The most notable is in the E1 helix (Figure 5B). In the apo-form, E1 extends by an extra turn that encompasses the 'x' and 'y' ligand-binding residues, Asp35 and Asp37, and clashes with the metal ion position in the Mg^{2+}-bound structure (Li et al., 2009) (Figure 5B). Additionally, apo-N-lobe EF1 and EF2 are further away from each

other and lack the short β-hairpin that connects them in the Mg^{2+}-bound structure (Figure 5B). These differences indicate that conformational changes, particularly in EF1, accompany metal binding and are consistent with divalent-ion induced chemical shift changes (Wingard et al., 2005). Although there are some differences in packing, the N-lobe hydrophobic core is buried in both forms (Figure S3B) and does not undergo large changes in exposure seen in the classic apo➔Ca^{2+}/CaM transition (Gifford et al., 2007; Grabarek, 2006) or in the CaBP1 apo➔Ca^{2+}/C-lobe transition (Li et al., 2009). The lack of large divalent ion induced conformational changes agrees with the absence of EF1 D➔A functional effects (Figures 4A and B) and suggests that N-lobe metal binding is unnecessary for CaBP1-mediated $Ca_V1.2$ modulation.

CaBP1 Ca^{2+}/C-lobe is similar to the NMR structure ($RMSD_{C\alpha}$ = 1.3Å over 60 Cα positions) (Figure 5C) and resembles the Ca^{2+}/CaM C-lobe 'open' conformation. The structural similarity is even better when compared to Ca^{2+}/CaM crystal structures regardless of whether the comparison is made with Ca^{2+}/CaM C-lobe alone (Wilson and Brunger, 2000) or bound to a target such as the $Ca_V1.2$ IQ domain (Van Petegem et al., 2005), ($RMSD_{C\alpha}$ =1.0 Å over 60 Cα positions for each) (Figure 5D). This similarity extends to many of the hydrophobic pocket sidechains. Consequently, the CaBP1 Ca^{2+}/C-lobe hydrophobic pocket appears ready to engage the $Ca_V1.2$ IQ domain in a manner similar to CaM Ca^{2+}/C-lobe (Van Petegem et al., 2005).

The most striking aspect of the structure is the well-ordered interlobe linker (Figures 5A and S3C), which is clamped to the N-lobe by insertion of Glu94 into a largely hydrophobic N-lobe cleft lined by Tyr56 and Leu91 (Figure 5E). This interaction is absent from the NMR structure (Li et al., 2009). Within the N-lobe cleft, the Glu94 sidechain is within hydrogen bonding distance of the Met54 backbone carbonyl oxygen. Comparison of non-crystallographically related asymmetric unit monomers reveals that the single helical turn in the C-terminal half of the linker (residues 95-99) forms a hinge point for a 5° rotation between the lobes (Figure S3D) and indicates that even in the compact state there is flexibility between the lobes.

Ca^{2+}/C-$lobe_{BP}$ and Ca^{2+}/C-$lobe_{CaM}$-IQ domain binding sites overlap

MMB and BBM chimeras having swapped CaBP1 and CaM C-lobes retain the properties of the parent, suggesting that CaBP1 and CaM C-lobes are functionally interchangeable (Figure 1). This, together with the strong structural similarity between Ca^{2+}/C-$lobe_{BP}$ and Ca^{2+}/C-$lobe_{CaM}$ bound to the $Ca_V1.2$ IQ domain (Figure 5D) and the prior evidence that CaBP1 acts by competing with CaM for the IQ domain (Zhou et al., 2004) led us to wonder whether CaBP1 and CaM Ca^{2+}/C-lobes interact with the $Ca_V1.2$ IQ domain at a common site. Titration of Ca^{2+}/C-$lobe_{BP}$ into a pre-formed Ca^{2+}/C-$lobe_{CaM}$-$Ca_V1.2$ IQ domain complex shows that Ca^{2+}/C-$lobe_{CaM}$ blocks binding of Ca^{2+}/C-$lobe_{BP}$ (Figure 6A) and supports the idea that the high affinity $Ca_V1.2$ IQ domain binding sites for each overlap. To explore this possibility further, we examined the effects of alanine mutations at F1628 and F1631, two residues that serve as anchors for Ca^{2+}/C-$lobe_{CaM}$-$Ca_V1.2$ IQ domain interactions (Van Petegem et al., 2005).

ITC experiments with Ca^{2+}/C-$lobe_{BP}$ and the F1628A peptide at 15°C, the temperature of our other ITC analyses, gave a small, endothermic signal (Figure 6B). Therefore, we evaluated Ca^{2+}/C-$lobe_{BP}$ binding to the F1628A peptide at 25°C, where the signal was robust (Figure 6C) and compared the results to titration of Ca^{2+}/C-$lobe_{BP}$ into the wild-type peptide at the same temperature (Figure 6D). The data show that $Ca_V1.2$ F1628A reduced Ca^{2+}/C-$lobe_{BP}$ affinity and binding enthalpy by ~48-fold and ~4 kcal mol^{-1}, respectively. The enthalpy reduction magnitude is similar to that caused by F1628A for Ca^{2+}/C-$lobe_{CaM}$ (Van Petegem et al., 2005) and is consistent with a loss of hydrophobic interactions.

Measurements with the F1631A peptide (Figure 6E) showed a ~33-fold and ~0.6 kcal mol^{-1} reduction in affinity and binding enthalpy, respectively. The F1631A change also reduces binding affinity and enthalpy for Ca^{2+}/C-lobe$_{CaM}$ (Figure 6F). Taken together, these experiments strongly support the idea that CaBP1 Ca^{2+}/C-lobe interacts with the $Ca_V1.2$ IQ domain in a manner akin to Ca^{2+}/CaM C-lobe (Fallon et al., 2005; Van Petegem et al., 2005).

Interlobe linker Glu94 is essential for CDI inhibition but not $Ca_V1.2$ IQ domain binding

Given that the CaBP1 interlobe linker is well ordered, makes specific interactions with the N-lobe, and is crucial to CDI inhibition, we used an alanine scan to investigate the functional contribution of each residue. Each alanine mutation diminished CDI inhibition (Figure 7A and B); however, E94A was the only change that completely eliminated CDI inhibition (Figure 7A and B). E94A also caused the appearance of CDI tachyphylaxis (Figure 7C and D) resulting from changes in recovery from inactivation similar to the DMIG linker mutant (Figure S4). To explore the importance of the Glu94 position further, we tested the effects of E94Q and E94D. E94Q almost completely eliminated CDI inhibition (Fig 7A and B) whereas, E94D allowed partial CDI inhibition. These results indicate that the sidechain carboxylate and precise sidechain geometry are essential. To probe the N-lobe/Glu94 interaction further, we replaced Tyr56, which contributes many N-lobe pocket/Glu94 contacts, with alanine. This change substantially diminishes CDI inhibition (Figure 7E and Table 1) and further supports the importance of the N-lobe/Glu94 interaction. The paramount functional role for Glu94 agrees well with the structurally defined N-lobe/Glu94 interaction (Figure 5E).

Despite the effects that E94A had on function, ITC experiments revealed that the loss of the N-lobe/Glu94 interaction caused by E94A altered ΔH and ΔS but spared the affinity for the $Ca_V1.2$ IQ domain (K_d = 0.336 ± 0.097 nM, Table 2, Figure S5). This result prompted us to test whether the ordered nature of the linker was a key element of CaBP1 function. We made a mutant (4G) that maintained the N-lobe/Glu94 interaction but that converted the C-terminal half of the linker (residues 97-100) to polyglycine. In contrast to the devastating effect of E94A, 4G retained an ability to inhibit CDI that was on par with the single alanine mutants (Figure 7F). Thus, although both the Glu94/N-lobe interaction and interlobe linker length (Figure 2) are essential for CaBP1 function, the order seen in the C-terminal half is not.

CaBP1 and CaM mediated CDF are two distinct processes

CaM-mediated $Ca_V1.2$ CDF requires $Ca_V\beta$ (Findeisen and Minor, 2009; Grueter et al., 2006; Hudmon et al., 2005) and CaMKII (Anderson et al., 1994; Grueter et al., 2006; Hudmon et al., 2005; Yuan and Bers, 1994). Although CaMKII activation is not necessary for CaBP1-mediated CDF (Zhou et al., 2004), the extent to which $Ca_V1.2$ CaM-mediated CDF (Van Petegem et al., 2005; Zühlke et al., 1999; Zühlke et al., 2000) and CaBP1-mediated CDF (Zhou et al., 2004) share molecular requirements has remained unclear. To test whether CaBP1-mediated CDF necessitates the presence of $Ca_V\beta$, we used a $Ca_V1.2$ mutant, 'HotA', that cannot bind $Ca_V\beta$ (Van Petegem et al., 2008) and that eliminates CaM-mediated CDF (Findeisen and Minor, 2009). Unlike the case with CaM, CaBP1 supports CDF when co-expressed with $Ca_V1.2$ HotA or wild-type $Ca_V1.2$ in the absence of $Ca_V\beta_{2a}$ (Figure 8A and B). Thus, CaBP1-mediated CDF does not require $Ca_V\beta$.

$Ca_V1.2$ CaM-mediated CDF is unmasked by the $Ca_V1.2$ IQ domain mutation, I1624A (Van Petegem et al., 2005; Zühlke et al., 1999; Zühlke et al., 2000) (Figure 8A and B). If CaBP1-mediated CDF were similar to CaM-mediated CDF, one might expect that I1624A would enhance CaBP1-mediated CDF. Contrary to this expectation, co-expression of $Ca_V1.2$

I1624A with CaBP1 produces CDF having a magnitude indistinguishable from that seen with CaBP1 and $Ca_V1.2$ (Figure 8A and B). $Ca_V1.2$ IQ domain residues F1618, Y1619, and F1622 are involved in Ca^{2+}/CaM N-lobe-IQ domain interactions that play a role in $Ca_V1.2$ CaM-mediated CDF (Hudmon et al., 2005; Van Petegem et al., 2008). The triple alanine mutant, F1618A/Y1619A/F1622A, ('TripleA'), eliminates CaM-mediated CDF (Van Petegem et al., 2008). In contrast, TripleA had no effect on CaBP1 mediated CDF (Figure 8A and B) or on CaBP1 CDI inhibition (Figure 8C). The insensitivity of CaBP1-medated CDF to manipulations that affect CaM-mediated CDF demonstrates that $Ca_V1.2$ CaM-mediated CDF and $Ca_V1.2$ CaBP1-mediated CDF are different and indicates that their underlying molecular mechanisms are different.

Discussion

CaBPs belong to a large calcium sensor family found throughout the nervous system (Burgoyne et al., 2004; Haeseleer et al., 2002; Weiss and Burgoyne, 2002) and closely resemble CaM (Haeseleer et al., 2002; Weiss and Burgoyne, 2002). Accordingly, CaBPs interact with diverse classes of CaM-modulated proteins (Haynes et al., 2006): Ca_Vs (Lee et al., 2002; Yang et al., 2002; Zhou et al., 2004), IP3 Receptors (Kasri et al., 2004; White et al., 2006; Yang et al., 2002), TRP channels (Kinoshita-Kawada et al., 2005), and myosin 1c (Tang et al., 2007). CaBP-target interactions impart functional changes distinct from those caused by CaM (Kasri et al., 2004; Lee et al., 2002; Yang et al., 2002; Zhou et al., 2004) and may diversify neuronal responses to calcium signals. CaBPs interact with and reshape the functional properties of certain Ca_Vs (Cui et al., 2007; Haeseleer et al., 2004; Lee et al., 2002; Tippens and Lee, 2007; Yang et al., 2006; Zhou et al., 2004). Because Ca_Vs are prominent in cellular calcium signaling pathways (Clapham, 2007), CaBP remodeling of Ca_V activity should reach well beyond electrical excitation properties.

CDI is an important type of Ca_V feedback modulation that limits cellular calcium entry in response to electrical activity. There are a number of situations in which CDI is overridden (Striessnig, 2007). One mechanism is CaBP1 substitution for CaM within Ca_V multiprotein complexes in retinal (Haeseleer et al., 2004) and auditory (Cui et al., 2007; Yang et al., 2006) neurons. This component change also happens in the brain (Zhou et al., 2004), blocks CDI in $Ca_V1.2$ and $Ca_V1.3$ (Cui et al., 2007; Yang et al., 2006; Zhou et al., 2004; Zhou et al., 2005), and introduces CDF to $Ca_V1.2$ (Zhou et al., 2004). CaBP1 and CaM have two independently-folded EF-hand containing lobes separated by a linker (Li et al., 2009; Masino et al., 2000; Tsalkova and Privalov, 1985). This likeness presents the question of which elements endow CaBP1 with the ability to alter $Ca_V1.2$ behavior differently from CaM. Our chimera-based analysis eliminated a role for CaBP1 N-terminal myristoylation, which is important for $Ca_V2.1$ modulation (Few et al., 2005), and identified the N-lobe and interlobe linker as the elements that allow CaBP1 to inhibit CDI and enable CDF in $Ca_V1.2$ (Figure 1).

The ability of CaBP1 C-lobe to bind calcium was important but not integral to CDI inhibition. This lack of sensitivity would seem to conflict with the reported calcium-dependency of the CaBP1-$Ca_V1.2$ IQ domain interaction (Zhou et al., 2004). However, the ability of CaBP1-EF3, EF4, and EF34 mutants to block CDI is reminiscent of the ability of the CaM EF34 mutant to block CDI (Peterson et al., 1999) and suggests that part of the CaBP1 CDI inhibition mechanism could arise from simple competition with apo-CaM binding to $Ca_V1.2$. Nevertheless, this effect cannot embody the entire mechanism. Our data show that only the BBM chimera but not BMM or MBM chimeras or the E94A mutant block CDI. If competition were the only effect, these mutants would be potent CDI inhibitors. Thus, the data strongly suggest that besides CaM competition, there must be an

active role for the CaBP1 N-lobe/Glu94 module in $Ca_V1.2$ CDI inhibition and this role is the dominant contributor.

The CaBP1 crystal structure revealed an unanticipated N-lobe/Glu94 interaction (Figure 5E) that is indispensible for CaBP1 CDI inhibition and CaBP1-mediated CDF of $Ca_V1.2$ (Figure 7). It is notable that this position is conserved CaBP2, CaBP4, and CaBP5 (Figure S2), particularly as CaBP4 inhibits $Ca_V1.3$ CDI (Cui et al., 2007; Yang et al., 2006). Thus, in addition to serving as part of the CaBP1 module required for $Ca_V1.2$ CDI inhibition, the N-lobe/Glu94 interaction may have a role in other CaBPs.

The $Ca_V1.2$ IQ domain is the essential CaM modulation site (Peterson et al., 1999; Pitt et al., 2001) and main CaBP1 binding site (Zhou et al., 2004). Our data uncover a strong structural similarity between the CaM and CaBP1 Ca^{2+}/C-lobes (Figure 5D). This structural mimicry suggests that both bind the $Ca_V1.2$ IQ domain in a similar manner. This idea is supported by the interchangeability of CaBP1 and CaM C-lobes with respect to parent molecule $Ca_V1.2$ modulation (Figures 1D-G) and is consistent with the similar functional sensitivity of both proteins to $Ca_V1.2$ IQ domain mutations (Zhou et al., 2004). Further, our ITC studies reveal that Ca^{2+}/C-lobe$_{BP}$ and Ca^{2+}/C-lobe$_{CaM}$ bind with similar affinities to a mutually exclusive $Ca_V1.2$ IQ domain site (Figure 6A, C and D, Table 2) and that mutations of residues that form anchors for Ca^{2+}/C-lobe$_{CaM}$ greatly diminish the ability of Ca^{2+}/C-lobe$_{BP}$ to bind (Figure 6C-F). Together, these results suggest that CaBP1 and CaM C-terminal lobes have the same main function, formation of high affinity attachment to the $Ca_V1.2$ IQ domain and that this attachment site overlaps.

ITC experiments with full-length CaBP1 show that it binds the $Ca_V1.2$ IQ domain ~40-fold stronger than Ca^{2+}/C-lobe$_{BP}$ and that the CaBP1 E94A mutation, which eliminates CDI inhibition, has no effect on binding affinity. Superposition of the Ca^{2+}/CaBP1 and Ca^{2+}/CaM C-lobes in the context of the Ca^{2+}/CaM-$Ca_V1.2$ IQ domain complex (Van Petegem et al., 2005) indicates that the compact CaBP1 conformation observed in the crystal structure is incompatible with $Ca_V1.2$ IQ domain binding. Many CaBP1 N-lobe/Glu94 atoms clash with the $Ca_V1.2$ IQ helix (Figure S6). Therefore, although there is good evidence that the Ca^{2+}/CaBP1 C-lobe binds the $Ca_V1.2$ IQ domain in a mode similar to Ca^{2+}/CaM C-lobe, CaBP1 binding must involve a conformation in which the CaBP1 N-lobe is in different position than seen in the CaBP1 structure.

Our ITC experiments indicate that the CaBP1 N-lobe participates in $Ca_V1.2$ IQ domain binding. If CaBP1 Ca^{2+}/C-lobe and CaM Ca^{2+}/C-lobe bind the $Ca_V1.2$ IQ domain similarly, one candidate CaBP1 N-lobe interaction site would be the $Ca_V1.2$ IQ domain residues that comprise the CaM Ca^{2+}/N-lobe binding site (F1618, Y1619, and F1622) (Fallon et al., 2005; Van Petegem et al., 2005). Nevertheless, functional analysis of the $Ca_V1.2$ TripleA mutant, which disrupts these anchors and eliminates CaM-mediated CDF (Van Petegem et al., 2005), reveals that neither CaBP1-mediated CDF or CDI inhibition depend on these residues. Therefore, CaBP1 N-lobe must interact with $Ca_V1.2$ differently than Ca^{2+}/CaM N-lobe. Conformational differences between the CaBP1 crystal and solution structures (Li et al., 2009) show that CaBP1 can adopt various interlobe conformations. Further, CaBP1 modulation of $Ca_V1.2$ tolerates substitutions that render the C-terminal part of the interlobe linker maximally flexible (Figure 7F). Thus, we propose that the CaBP1 binds the $Ca_V1.2$ IQ domain using a similar C-lobe position to CaM but an alternate N-lobe pose such as an open structure that would maintain the CaBP1 N-lobe/Glu94 interaction but flex in the C-terminal portion of the interlobe linker. This could allow CaBP1 to interact with the $Ca_V1.2$ cytoplasmic N-terminal domain, a channel element that has the capacity to bind CaBP1 and that is required for CaBP1 modulation of $Ca_V1.2$ (Zhou et al., 2005).

CaBP1 affects Ca_V1s and Ca_V2s differently. CaBP1 inhibits $Ca_V1.2$ and $Ca_V1.3$ CDI (Cui et al., 2007; Yang et al., 2006; Zhou et al., 2004; Zhou et al., 2005), whereas it accelerates $Ca_V2.1$ CDI and changes activation (Few et al., 2005; Lee et al., 2002). Additionally, CaBP1 blocks $Ca_V2.1$ CDF (Few et al., 2005; Lee et al., 2002). These $Ca_V2.1$ functional changes require CaBP1 N-terminal myristoylation (Few et al., 2005), a modification that we find irrelevant for CaBP1 modulation of $Ca_V1.2$. This result is corroborated the ability of a non-myristyolated CaBP1 splice variant, caldendrin, to block $Ca_V1.2$ CDI (Tippens and Lee, 2007). The mechanistic basis for the difference between $Ca_V1.2$ and $Ca_V2.1$ modulation by CaBP1 remains unresolved. CDI and CDF in Ca_V1s and Ca_V2s arise from the actions of different CaM lobes (Dunlap, 2007) that are correlated with different Ca^{2+}/CaM binding modes on the Ca_V1 (Van Petegem et al., 2005) and Ca_V2 (Kim et al., 2008) IQ domains (however, *cf.*, (Mori et al., 2008)). Similar to Ca^{2+}/CaM (Kim et al., 2008; Van Petegem et al., 2005), we find that both CaBP1 lobes can bind the IQ domain. It is tempting to speculate that the differential effects of CaBP1 on Ca_V1 and Ca_V2 CDI and CDF and the differential effects of the CaM lobes with respect to the same processes are related. CaBP1 also binds other CaM binding channel segments (Dick et al., 2008; Ivanina et al., 2000; Lee et al., 1999). It is possible that the differential effects also require interactions with these or other channel domains. Delineating how CaBPs act should not only unravel CaBP-specific mechanisms, but may help dissect the still imperfectly understood action of CaM with respect to CDI and CDF. Our data provide the framework for investigation of these issues.

We have identified the features that allow CaBP1 to modulate $Ca_V1.2$ differently from CaM. Our studies reveal an unanticipated essential role for the interlobe linker and show that CaBP1 has two structural modules that encode two separate functions. CaBP1 C-lobe serves as the IQ domain anchor, whereas the N-lobe/linker module contains the elements required for channel modulation. The elements comprising the N-lobe/Glu94 interaction are conserved in many CaBPs that interact with diverse targets. Thus, the structural underpinnings outlined here are likely to aid understanding how CaBPs act on a wide range of targets that have dual modulation by CaM and CaBPs.

Experimental procedures

Expression and Purification

Individual human CaBP1-S (AF169148) lobes were expressed as fusion proteins from a pET28 vector denoted ‘HMT’ (Van Petegem et al., 2004) in *E. coli* BL21(DE3)pLysS. CaBP1(Δ2-15) and CaBP1(Δ2-15) K130A, and selenium methionine substituted CaBP1(Δ2-15) K130A were expressed a pEGST vector in *E. coli* BL21(DE3)pLysS. $Ca_V1.2$ IQ domains were made as described previously (Van Petegem et al., 2005). Expression and purification details can be found in Supplementary Experimental Procedures.

Crystallization and Refinement

CaBP1(Δ2-15) was crystallized by hanging drop vapor diffusion at 20°C from equal volumes of protein in buffer A and well solution containing 1.9 M $(NH_4)_2SO_4$, 2-4 % 1,2-propanediol and 0.1 M citrate/sodium citrate, pH 5.5. Native and selenomethionine-substituted CaBP1(Δ2-15) K130A were crystallized similarly except that 1,2-propanediol was replaced by 5-7 % 1,6-hexanediol. Crystals were flash-frozen in well solution plus 20% glycerol. Diffraction data were collected at Beamline 8.3.1 (Advanced Light Source, Lawrence Berkeley National Laboratories) and processed using MOSFLM 7.0.4 (Leslie, 1992). A three-wavelength MAD experiment was performed on crystals of SeMet-substituted CaBP1(Δ2-15) K130A. 64 initial selenium positions were located using SHELXD (Uson and Sheldrick, 1999). After phasing and density modification using DM, the resulting electron density allowed building of an initial model that was improved by

iterative cycles of manual building and refinement against native data using Refmac5 (Collaborative Computational Project, 1994). TLS-tensors were used throughout refinement. Tight NCS restraints were employed initially and relaxed in later refinement cycles. Each final model consists of six CaBP1 monomers.

Isothermal titration calorimetry

Titrations were performed at 15°C or 25°C using a VP-ITC Microcalorimeter (MicroCal). Samples were dialyzed overnight at 4°C (Slide-A-Lyzer, 3.5 kDa molecular weight cut-off, Thermo Scientific) against 5 mM KCl, 1 mM $CaCl_2$, 10 mM Hepes, pH 7.4. After centrifugation (30′, 70,000 × g, 4 °C) protein concentrations were determined by absorbance at 280 nm (Edelhoch, 1967). All samples were degassed for 5− prior to loading into the VP-ITC. $Ca_V1.2$ IQ domain peptide at concentrations of 5.5 or 7.5 μM were titrated with 75 μM CaBP1 constructs using a schedule of one 4 μl titrant injection followed by 29 injections of 10 μl. For competition experiments, 7.5 μM $Ca_V1.2$ IQ domain peptide was preincubated with 50 μM of Ca^{2+}/N-$lobe_{BP}$ and titrated with a solution of 75 μM of CaBP1. To correct the baseline, either heat of dilution from titrations of injectant into buffer was subtracted (Figures 3A and 3D) or the final titration points were used to estimate the baseline (Figures 3B, 3F-H). Data were processed with MicroCal Origin 7.0 using a single site binding model or a competitive binding model, where appropriate.

For binding isotherm analysis of the simultaneous addition of Ca^{2+}/N-$lobe_{BP}$ and Ca^{2+}/C-$lobe_{BP}$ to the $Ca_V1.2$ IQ domain, we used a modified version of competition ligand binding by displacement ITC (Sigurskjold, 2000) that takes into account both ligands are added simultaneously. Thus, the stoichiometric concentration of B in the calorimeter cell, equation [26] from (Sigurskjold, 2000), $[B]_{0,i} = f_{t,i}[B]_0$,, is replaced by $[B]_{0,i} = [B]_2 (1\text{-}f_{t,i})$, where $[B]_s$ is concentration of Ca^{2+}/N-$lobe_{BP}$ in the injection syringe and $f_{t,i}$ is the total dilution factor after the *i*th injection, respectively.

Electrophysiology

Human $Ca_V1.2$ (α_1C77, CAA84346) in pcDNA3.1 (Invitrogen), rat $Ca_V\beta_{2a}$ (NP 446303) in pGEMHE, and $Ca_V\alpha_2\delta$-1 (NM_00182276) in pcDNA3.1 were co-expressed with either *Homo sapiens* CaM (NM_006888) or the short isoform of human CaBP1-S (AF169148) in pGEMHE for *Xenopus* oocyte two-electrode voltage clamp experiments. Point mutations were introduced using QuikChange (Stratagene). For chimera construction, CaM and CaBP1 were divided into three elements: N-lobe (CaM 1-78 and CaBP1 1-92), linker (CaM 79-82 and CaBP1 93-100 for CaBP1), and C-lobe (CaM 83-149 and CaBP1 101-167). All chimeras having CaBP1 N-lobe include the N-terminal myristoylation domain. Inter-element junctions were framed by introduction of EcoRV sites generated using QuikChange. Elements were excised using EcoRV and either HindIII or XhoI present in the parent vector and combined to produce the chimeras. Following chimera generation, junction sites were returned to the native sequence using QuikChange.

After overnight linearization (XhoI for pcDNA3.1 and NheI for pGEMHE), capped mRNAs were synthesized (T7 mMessenger kit (Ambion)) according to the manufacturer's protocols. RNA concentrations were determined by A_{260nm}. 50 nl of $Ca_V\alpha_1$, $Ca_V\beta$, $Ca_V\alpha_2\delta$-1, and CaBP1 or CaM mRNA at a molar ratio of 1:1:1:20 were injected into defolliculated stage VI *Xenopus* oocytes using Nanoject II injector (Drummond Scientific). Oocytes were kept at 18 °C in ND96 medium containing penicillin and streptomycin. Two-electrode voltage-clamp experiments were performed 2 to 4 days post-injection using a GeneClamp 500B (Axon Instruments) amplifier controlled by a 1,200 MHz processor computer (Celeron, Gateway) running CLAMPEX 8.2.0.244, and digitized at 1kHz with a Digidata 1332A (Axon Instruments). Immediately prior to recording, oocytes were injected with 47 nl of 100 mM

BAPTA to minimize Ca^{2+}-activated Cl^- current. Recording solutions contained either 40 mM $Ba(OH)_2$ or 40 mM $Ca(NO_3)_2$, 50 mM NaOH, 1 mM KOH, and 10 mM HEPES, adjusted to pH 7.4 using HNO_3. Electrodes were filled with 3M KCl and had 0.3-2.0 MΩ resistances. Leak currents were subtracted using a P/4 protocol. Currents were analyzed with Clampfit 8.2 (Axon Instruments). Oocytes were superfused during recording using a Valvelink 16 controller (Automate Scientific). Holding potential for all experiments was −90mV. Results are from at least two independent oocyte batches. ti_{300} values were calculated from normalized currents at +20 mV and represent the percentage inactivation after 300 milliseconds. Inactivation τ values were calculated at a test potential of +20 mV as described (Findeisen and Minor, 2009). CDF was elicited by a train of 40, 50 ms pulses to +20 mV at 3Hz and calculated as the ratio of the peak current from the last pulse divided by the first. Recovery from inactivation was measured by a protocol with two 450 ms pulses to +20 mV separated by variable time intervals. Consecutive sweeps were separated by 30 s.

Pull-down experiments

Bacterial pellets from a 50 ml culture of CaBP1, CaBP1 mutants, CaM, or CaBP1/CaM chimeras co-expressed with HMT-tagged $Ca_V1.2$ IQ domain were resuspended in 1.6 ml lysis buffer (10% sucrose, 150 mM KCl, 5 mM $MgCl_2$, 1 mM $CaCl_2$, 25 μg/ml DNAaseI, 1 mM PMSF, 100 mM Tris, pH 8.8) and lysed by sonication. 100 μl amylose resin in buffer AmyA (250 mM KCl, 1 mM $CaCl_2$, 10 mM Hepes/KOH, pH 7.4) was incubated with the bacterial lysate for 30 minutes at 4 °C with gentle agitation. After four washes with 500 μl AmyA, bound material was eluted in 500 μl AmyA containing 10 mM maltose. Input and eluate fractions were analyzed by SDS-PAGE.

Supplementary Material

Refer to Web version on PubMed Central for supplementary material.

Acknowledgments

This work was supported by grants to DLM (NIH-NHLBI R01-HL080050 and the American Heart Association 0740019N) and to FF from the American Heart Association. We thank A. Lee for the CaBP1 clone; D. Palanivelu, A. Tolia, and F. Van Petegem for manuscript comments; J. Holton at ALS Beamline 8.3.1 for data collection assistance. DLM is an AHA Established Investigator. CaBP1 and CaBP1 K130A coordinates and structure factors are deposited with the RCSB under codes 3OX5 and 3OX6, respectively.

References

Alseikhan BA, DeMaria CD, Colecraft HM, Yue DT. Engineered calmodulins reveal the unexpected eminence of Ca2+ channel inactivation in controlling heart excitation. Proc Natl Acad Sci U S A. 2002; 99:17185–17190. [PubMed: 12486220]

Anderson ME, Braun AP, Schulman H, Premack BA. Multifunctional Ca2+/calmodulin-dependent protein kinase mediates Ca(2+)-induced enhancement of the L-type Ca2+ current in rabbit ventricular myocytes. Circ Res. 1994; 75:854–861. [PubMed: 7923631]

Burgoyne RD, O'Callaghan DW, Hasdemir B, Haynes LP, Tepikin AV. Neuronal Ca2+-sensor proteins: multitalented regulators of neuronal function. Trends Neurosci. 2004; 27:203–209. [PubMed: 15046879]

Catterall WA. Structure and regulation of voltage-gated Ca2+ channels. Annu Rev Cell Dev Biol. 2000; 16:521–555. [PubMed: 11031246]

Clapham DE. Calcium signaling. Cell. 2007; 131:1047–1058. [PubMed: 18083096]

Collaborative Computational Project, N. The CCP4 suite: Programs for protein crystallography. Acta Crystallogr D Biol Crystallogr. 1994; 50:760–763. [PubMed: 15299374]

Cui G, Meyer AC, Calin-Jageman I, Neef J, Haeseleer F, Moser T, Lee A. Ca2+-binding proteins tune Ca2+-feedback to Cav1.3 channels in mouse auditory hair cells. J Physiol. 2007; 585:791–803. [PubMed: 17947313]

Davies A, Hendrich J, Van Minh AT, Wratten J, Douglas L, Dolphin AC. Functional biology of the alpha(2)delta subunits of voltage-gated calcium channels. Trends Pharmacol Sci. 2007; 28:220–228. [PubMed: 17403543]

Derewenda ZS, Vekilov PG. Entropy and surface engineering in protein crystallization. Acta Crystallogr D Biol Crystallogr. 2006; 62:116–124. [PubMed: 16369101]

Dick IE, Tadross MR, Liang H, Tay LH, Yang W, Yue DT. A modular switch for spatial Ca2+ selectivity in the calmodulin regulation of CaV channels. Nature. 2008; 451:830–834. [PubMed: 18235447]

Dolphin AC. beta subunits of voltage-gated calcium channels. J Bioenerg Biomembr. 2003; 35:599–620. [PubMed: 15000522]

Dunlap K. Calcium channels are models of self-control. J Gen Physiol. 2007; 129:379–383. [PubMed: 17438121]

Edelhoch H. Spectroscopic determination of tryptophan and tyrosine in proteins. Biochemistry. 1967; 6:1948–1954. [PubMed: 6049437]

Erickson MG, Liang H, Mori MX, Yue DT. FRET two-hybrid mapping reveals function and location of L-type Ca2+ channel CaM preassociation. Neuron. 2003; 39:97–107. [PubMed: 12848935]

Fallon JL, Halling DB, Hamilton SL, Quiocho FA. Structure of calmodulin bound to the hydrophobic IQ domain of the cardiac Ca(v)1.2 calcium channel. Structure. 2005; 13:1881–1886. [PubMed: 16338416]

Fallon JL, Quiocho FA. A closed compact structure of native Ca(2+)-calmodulin. Structure. 2003; 11:1303–1307. [PubMed: 14527397]

Few AP, Lautermilch NJ, Westenbroek RE, Scheuer T, Catterall WA. Differential regulation of CaV2.1 channels by calcium-binding protein 1 and visinin-like protein-2 requires N-terminal myristoylation. J Neurosci. 2005; 25:7071–7080. [PubMed: 16049184]

Findeisen F, Minor DL Jr. Disruption of the IS6-AID Linker Affects Voltage-gated Calcium Channel Inactivation and Facilitation. J Gen Physiol. 2009; 133:327–343. [PubMed: 19237593]

Gifford JL, Walsh MP, Vogel HJ. Structures and metal-ion-binding properties of the Ca2+-binding helix-loop-helix EF-hand motifs. Biochem J. 2007; 405:199–221. [PubMed: 17590154]

Grabarek Z. Structural basis for diversity of the EF-hand calcium-binding proteins. J Mol Biol. 2006; 359:509–525. [PubMed: 16678204]

Grueter CE, Abiria SA, Dzhura I, Wu Y, Ham AJ, Mohler PJ, Anderson ME, Colbran RJ. L-type Ca2+ channel facilitation mediated by phosphorylation of the beta subunit by CaMKII. Mol Cell. 2006; 23:641–650. [PubMed: 16949361]

Haeseleer F, Imanishi Y, Maeda T, Possin DE, Maeda A, Lee A, Rieke F, Palczewski K. Essential role of Ca2+-binding protein 4, a Cav1.4 channel regulator, in photoreceptor synaptic function. Nat Neurosci. 2004; 7:1079–1087. [PubMed: 15452577]

Haeseleer F, Imanishi Y, Sokal I, Filipek S, Palczewski K. Calcium-binding proteins: intracellular sensors from the calmodulin superfamily. Biochem Biophys Res Commun. 2002; 290:615–623. [PubMed: 11785943]

Haeseleer F, Sokal I, Verlinde CL, Erdjument-Bromage H, Tempst P, Pronin AN, Benovic JL, Fariss RN, Palczewski K. Five members of a novel Ca(2+)-binding protein (CABP) subfamily with similarity to calmodulin. J Biol Chem. 2000; 275:1247–1260. [PubMed: 10625670]

Haynes LP, Fitzgerald DJ, Wareing B, O'Callaghan DW, Morgan A, Burgoyne RD. Analysis of the interacting partners of the neuronal calcium-binding proteins L-CaBP1, hippocalcin, NCS-1 and neurocalcin delta. Proteomics. 2006; 6:1822–1832. [PubMed: 16470652]

Hendrickson WA, Ogata CM. Phase Determination from Multiwavelength Anomolous Diffraction Measurements. Meth. Enzymol. 1997; 276:494–523.

Hudmon A, Schulman H, Kim J, Maltez JM, Tsien RW, Pitt GS. CaMKII tethers to L-type Ca2+ channels, establishing a local and dedicated integrator of Ca2+ signals for facilitation. J Cell Biol. 2005; 171:537–547. [PubMed: 16275756]

Ivanina T, Blumenstein Y, Shistik E, Barzilai R, Dascal N. Modulation of L-type Ca2+ channels by gbeta gamma and calmodulin via interactions with N and C termini of alpha 1C. J Biol Chem. 2000; 275:39846–39854. [PubMed: 10995757]

Kasri NN, Holmes AM, Bultynck G, Parys JB, Bootman MD, Rietdorf K, Missiaen L, McDonald F, De Smedt H, Conway SJ, et al. Regulation of InsP3 receptor activity by neuronal Ca2+-binding proteins. Embo J. 2004; 23:312–321. [PubMed: 14685260]

Kim EY, Rumpf CH, Fujiwara Y, Cooley ES, Van Petegem F, Minor DL Jr. Structures of CaV2 Ca2+/CaM-IQ domain complexes reveal binding modes that underlie calcium-dependent inactivation and facilitation. Structure. 2008; 16:1455–1467. [PubMed: 18940602]

Kinoshita-Kawada M, Tang J, Xiao R, Kaneko S, Foskett JK, Zhu MX. Inhibition of TRPC5 channels by Ca2+-binding protein 1 in Xenopus oocytes. Pflugers Arch. 2005; 450:345–354. [PubMed: 15895247]

Lautermilch NJ, Few AP, Scheuer T, Catterall WA. Modulation of CaV2.1 channels by the neuronal calcium-binding protein visinin-like protein-2. J Neurosci. 2005; 25:7062–7070. [PubMed: 16049183]

Lee A, Westenbroek RE, Haeseleer F, Palczewski K, Scheuer T, Catterall WA. Differential modulation of Ca(v)2.1 channels by calmodulin and Ca2+-binding protein 1. Nat Neurosci. 2002; 5:210–217. [PubMed: 11865310]

Lee A, Wong ST, Gallagher D, Li B, Storm DR, Scheuer T, Catterall WA. Ca2+/calmodulin binds to and modulates P/Q-type calcium channels. Nature. 1999; 399:155–159. [PubMed: 10335845]

Leslie AGW. Recent changes to the MOSFLM package for processing film and image plate data. Joint CCP4 + ESF-EAMCB Newsletter of Protein Crystallography. 1992; 26

Li C, Chan J, Haeseleer F, Mikoshiba K, Palczewski K, Ikura M, Ames JB. Structural insights into Ca2+-dependent regulation of inositol 1,4,5-trisphosphate receptors by CaBP1. J Biol Chem. 2009; 284:2472–2481. [PubMed: 19008222]

Masino L, Martin SR, Bayley PM. Ligand binding and thermodynamic stability of a multidomain protein, calmodulin. Protein Sci. 2000; 9:1519–1529. [PubMed: 10975573]

Mori MX, Vander Kooi CW, Leahy DJ, Yue DT. Crystal Structure of the Ca(V)2 IQ Domain in Complex with Ca(2+)/Calmodulin: High-Resolution Mechanistic Implications for Channel Regulation by Ca(2+). Structure. 2008; 16:607–620. [PubMed: 18400181]

Peterson BZ, DeMaria CD, Adelman JP, Yue DT. Calmodulin is the Ca2+ sensor for Ca2+ -dependent inactivation of L-type calcium channels. Neuron. 1999; 22:549–558. [PubMed: 10197534]

Pitt GS. Calmodulin and CaMKII as molecular switches for cardiac ion channels. Cardiovasc Res. 2007; 73:641–647. [PubMed: 17137569]

Pitt GS, Zühlke RD, Hudmon A, Schulman H, Reuter H, Tsien RW. Molecular basis of calmodulin tethering and Ca2+-dependent inactivation of L-type Ca2+ channels. J Biol Chem. 2001; 276:30794–30802. [PubMed: 11408490]

Rocque WJ, McWherter CA, Wood DC, Gordon JI. A comparative analysis of the kinetic mechanism and peptide substrate specificity of human and Saccharomyces cerevisiae myristoyl-CoA:protein N-myristoyltransferase. J Biol Chem. 1993; 268:9964–9971. [PubMed: 8486723]

Sigurskjold BW. Exact analysis of competition ligand binding by displacement isothermal titration calorimetry. Anal Biochem. 2000; 277:260–266. [PubMed: 10625516]

Striessnig J. C-terminal tailoring of L-type calcium channel function. J Physiol. 2007; 585:643–644. [PubMed: 18084049]

Tang N, Lin T, Yang J, Foskett JK, Ostap EM. CIB1 and CaBP1 bind to the myo1c regulatory domain. J Muscle Res Cell Motil. 2007; 28:285–291. [PubMed: 17994197]

Tippens AL, Lee A. Caldendrin, a neuron-specific modulator of Cav/1.2 (L-type) Ca2+ channels. J Biol Chem. 2007; 282:8464–8473. [PubMed: 17224447]

Tsalkova TN, Privalov PL. Thermodynamic study of domain organization in troponin C and calmodulin. J Mol Biol. 1985; 181:533–544. [PubMed: 3999139]

Uson I, Sheldrick GM. Advances in direct methods for protein crystallography. Curr Opin Struct Biol. 1999; 9:643–648. [PubMed: 10508770]

Van Petegem F, Chatelain FC, Minor DL Jr. Insights into voltage-gated calcium channel regulation from the structure of the CaV1.2 IQ domain-Ca2+/calmodulin complex. Nat Struct Mol Biol. 2005; 12:1108–1115. [PubMed: 16299511]

Van Petegem F, Clark KA, Chatelain FC, Minor DL Jr. Structure of a complex between a voltage-gated calcium channel beta-subunit and an alpha-subunit domain. Nature. 2004; 429:671–675. [PubMed: 15141227]

Van Petegem F, Duderstadt KE, Clark KA, Wang M, Minor DL Jr. Alanine-Scanning Mutagenesis Defines a Conserved Energetic Hotspot in the Ca(V)alpha(1) AID-Ca(V)beta Interaction Site that Is Critical for Channel Modulation. Structure. 2008; 16:280–294. [PubMed: 18275819]

Van Petegem F, Minor DL. The structural biology of voltage-gated calcium channel function and regulation. Biochem Soc Trans. 2006; 34:887–893. [PubMed: 17052221]

Weiss JL, Burgoyne RD. Sense and sensibility in the regulation of voltage-gated Ca(2+) channels. Trends Neurosci. 2002; 25:489–491. [PubMed: 12220869]

White C, Yang J, Monteiro MJ, Foskett JK. CIB1, a ubiquitously expressed Ca2+-binding protein ligand of the InsP3 receptor Ca2+ release channel. J Biol Chem. 2006; 281:20825–20833. [PubMed: 16723353]

Wilson MA, Brunger AT. The 1.0 A crystal structure of Ca(2+)-bound calmodulin: an analysis of disorder and implications for functionally relevant plasticity. J Mol Biol. 2000; 301:1237–1256. [PubMed: 10966818]

Wingard JN, Chan J, Bosanac I, Haeseleer F, Palczewski K, Ikura M, Ames JB. Structural analysis of Mg2+ and Ca2+ binding to CaBP1, a neuron-specific regulator of calcium channels. J Biol Chem. 2005; 280:37461–37470. [PubMed: 16147998]

Yang J, McBride S, Mak DO, Vardi N, Palczewski K, Haeseleer F, Foskett JK. Identification of a family of calcium sensors as protein ligands of inositol trisphosphate receptor Ca(2+) release channels. Proc Natl Acad Sci U S A. 2002; 99:7711–7716. [PubMed: 12032348]

Yang PS, Alseikhan BA, Hiel H, Grant L, Mori MX, Yang W, Fuchs PA, Yue DT. Switching of Ca2+-dependent inactivation of Ca(v)1.3 channels by calcium binding proteins of auditory hair cells. J Neurosci. 2006; 26:10677–10689. [PubMed: 17050707]

Yuan W, Bers DM. Ca-dependent facilitation of cardiac Ca current is due to Ca-calmodulin-dependent protein kinase. Am J Physiol. 1994; 267:H982–993. [PubMed: 8092302]

Zhou H, Kim SA, Kirk EA, Tippens AL, Sun H, Haeseleer F, Lee A. Ca2+-binding protein-1 facilitates and forms a postsynaptic complex with Cav1.2 (L-type) Ca2+ channels. J Neurosci. 2004; 24:4698–4708. [PubMed: 15140941]

Zhou H, Yu K, McCoy KL, Lee A. Molecular mechanism for divergent regulation of Cav1.2 Ca2+ channels by calmodulin and Ca2+-binding protein-1. J Biol Chem. 2005; 280:29612–29619. [PubMed: 15980432]

Zühlke RD, Pitt GS, Deisseroth K, Tsien RW, Reuter H. Calmodulin supports both inactivation and facilitation of L-type calcium channels. Nature. 1999; 399:159–162. [PubMed: 10335846]

Zühlke RD, Pitt GS, Tsien RW, Reuter H. Ca2+-sensitive inactivation and facilitation of L-type Ca2+ channels both depend on specific amino acid residues in a consensus calmodulin-binding motif in the(alpha)1C subunit. J Biol Chem. 2000; 275:21121–21129. [PubMed: 10779517]

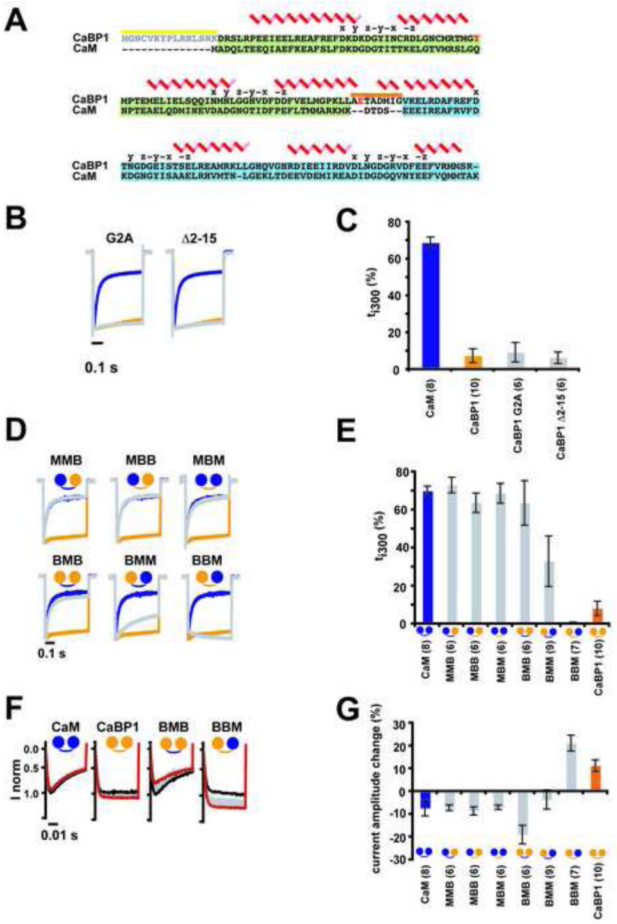

Figure 1.

CaBP1-CaM chimeras demonstrate the importance of the N-lobe and interlobe linker. **A**, Structure based alignment of CaBP1 and CaM. N-lobe and C-lobe are shaded green and blue, respectively. CaBP1 N-terminal myristoylation segment and interlobe linker are indicated by the yellow and orange bars, respectively. EF hand positions are indicated above the sequence according to standard nomenclature (Gifford et al., 2007). Secondary structure elements are indicated. CaBP1 residues Y56 and E94 are highlighted in red. **B**, CaBP1-mediated CDI inhibition is unaffected by myristoylation site mutants. Representative normalized I_{Ca} traces at a test potential of +20 mV for $Ca_V1.2$ expressed with $Ca_V\beta_{2a}$ and CaBP1 myristoylation mutants G2A and Δ2-15 (grey), CaBP1 (orange), or CaM (blue). **C,** t_{i300} values for data from '**B**'. **D,** Representative normalized I_{Ca} traces at a test potential of +20 mV for $Ca_V1.2$ expressed with $Ca_V\beta_{2a}$ and CaBP1-CaM chimeras (grey), wild-type CaBP1 (orange), or CaM (blue). Icons show the origin of the domain elements: CaBP1 (orange), CaM (blue). Chimeras containing CaBP1 N-lobe all contain the myristoylation domain. **E**, t_{i300} values for data from '**D**'. **F,** Relative current amplitude changes of I_{Ca} in response to 40 +20 mV pulses delivered at 3 Hz for $Ca_V1.2$ expressed with $Ca_V\beta_{2a}$ and the indicated chimeras. First (black), last (red) and every fourth trace (grey) are shown. **G,** Relative current changes between the last and first pulse for $Ca_V1.2$ expressed with $Ca_V\beta_{2a}$ and CaBP1, CaM, or the indicated chimeras. Parentheses indicate the number of oocytes tested. Error bars indicate s.d. See also Figures S1 and S2.

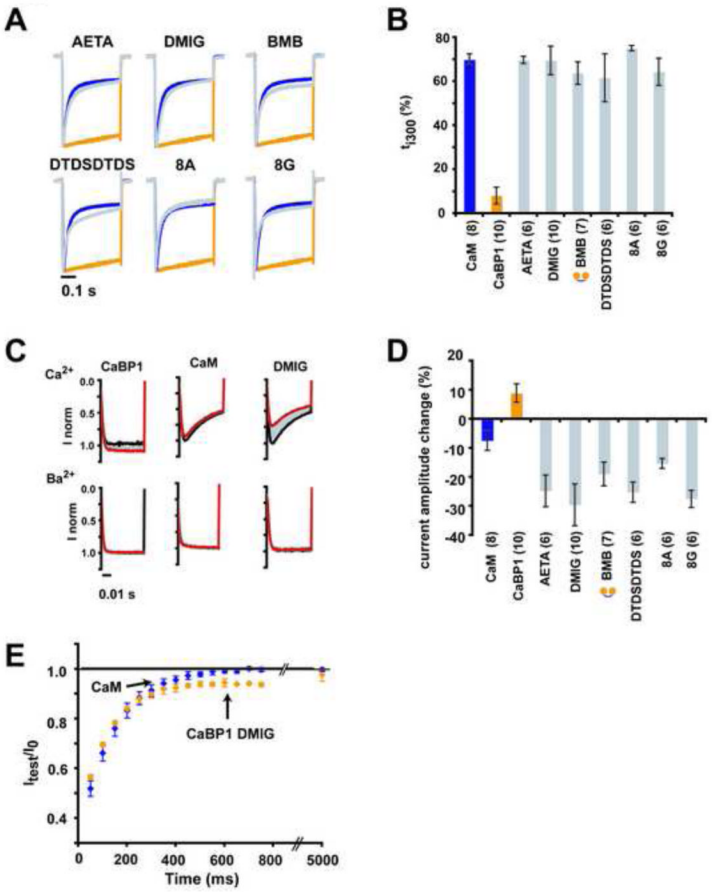

Figure 2.

Interlobe linker length and sequence have a crucial role in CaBP1 function. **A**, Representative normalized I_{Ca} traces at a test potential of +20 mV for $Ca_V1.2$ expressed with $Ca_V\beta_{2a}$ and indicated CaBP1 linker mutants (grey), CaBP1 (orange), or CaM (blue). **B**, t_{i300} values for data from '**A**'. BMB values are from Figure 1. **C,** Relative current amplitude changes of I_{Ca} and I_{Ba} in response to 40 +20 mV pulses delivered at 3 Hz for $Ca_V1.2$ expressed with $Ca_V\beta_{2a}$ and CaBP1, CaM, or the DMIG linker mutant. First (black), last (red) and every fourth trace (grey) are shown. **D**, Averaged frequency dependent change of I_{Ca} current amplitude for $Ca_V1.2$ expressed with $Ca_V\beta_{2a}$ and CaBP1, CaM, or the indicated linker mutants. **E**, Comparison of I_{Ca} recovery from inactivation for $Ca_V1.2$ expressed with $Ca_V\beta_{2a}$ and CaM (blue) or the CaBP1 DMIG linker mutant (orange) in response to two 450 ms pulses to +20 mV separated by variable time intervals. Parentheses indicate the number of oocytes tested. Error bars indicate s.d. See also Figures S1 and S2.

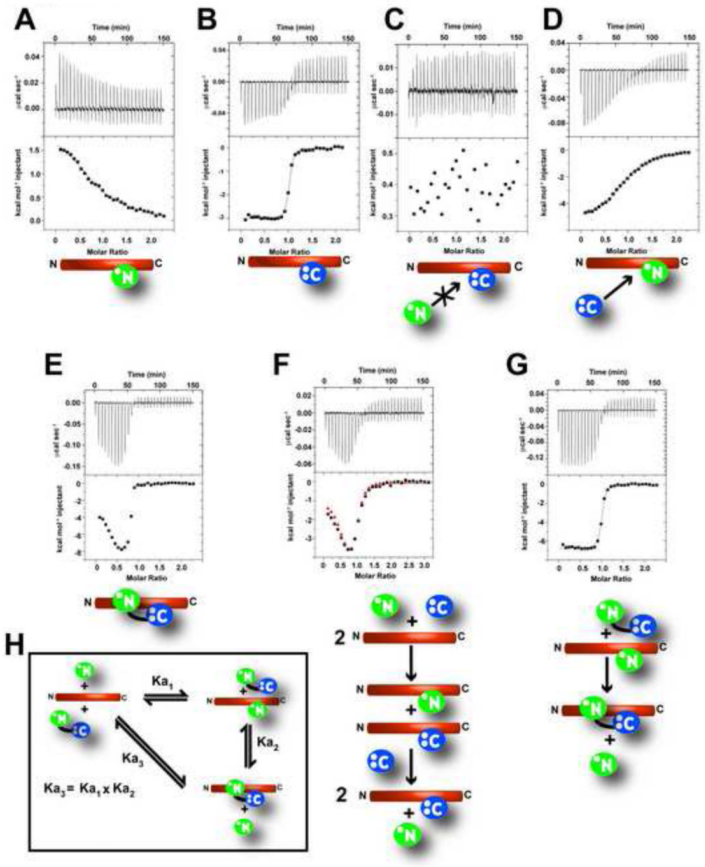

Figure 3.

Characterization of Ca^{2+}/CaBP1-$Ca_V1.2$ IQ domain interactions. Exemplar ITC titrations for: **A**, 75 μM Ca^{2+}/N-$lobe_{BP}$ into 7.5 μM IQ domain. **B**, 75 μM Ca^{2+}/C-$lobe_{BP}$ into 7.5 μM IQ domain. **C**, 75 μM Ca^{2+}/N-$lobe_{BP}$ into 7.5 μM $Ca_V1.2$ IQ domain and 11.25 μM Ca^{2+}/C-$lobe_{BP}$. **D,** 75 μM Ca^{2+}/C-$lobe_{BP}$ into 7.5 μM IQ domain and 50 μM Ca^{2+}/N-$lobe_{BP}$. **E,** 75 μM Ca^{2+}/CaBP1 into 5.5 μM IQ domain. **F,** 75 μM Ca^{2+}/C-$lobe_{BP}$ and 75 μM Ca^{2+}/N-$lobe_{BP}$ into 7.5 μM IQ domain. Red squares denote estimates of enthalpy changes using binding parameters derived from the single lobe binding.**G**, 75 μM Ca^{2+}/CaBP1 into 7.5 μM IQ domain and 50 μM Ca^{2+}/N-$lobe_{BP}$. **H,** Thermodyamic cycle for analysis of the binding of CaBP1 (Ka_3) to the $Ca_V1.2$ IQ domain. Ka_1 describes Ca^{2+}/N-$lobe_{Bp}$ binding. Ka_2 describes the competition of Ca^{2+}/N-$lobe_{BP}$ by CaBP1. Cartoons depict the observed binding reactions.

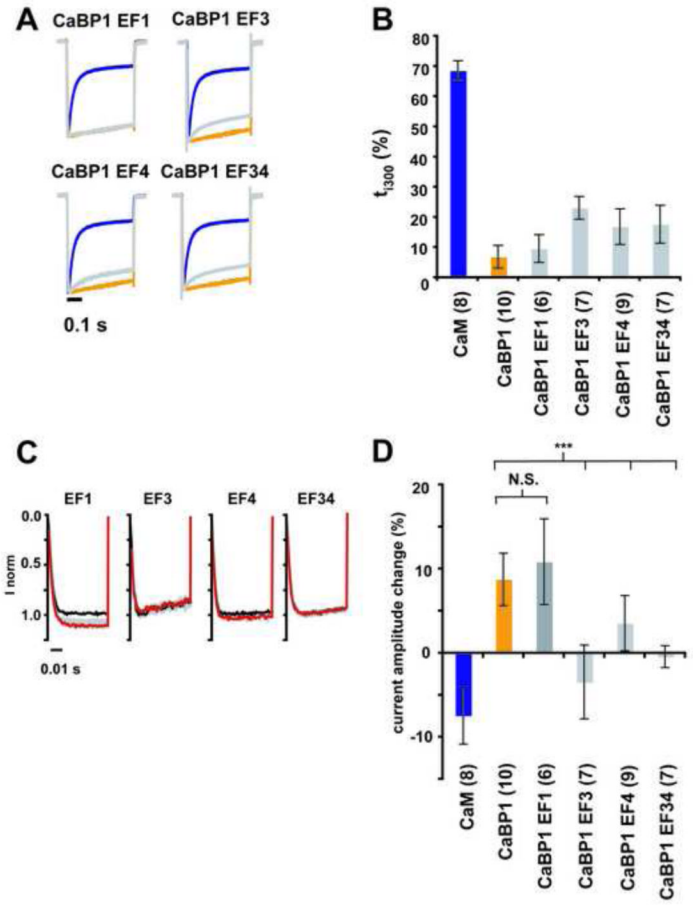

Figure 4.

C-terminal EF-hands are required for CaBP1-mediated CDF but not for inhibition of CDI. **A**, Representative normalized I_{Ca} traces at a test potential of +20 mV for $Ca_V1.2$ expressed with $Ca_V\beta_{2a}$ and indicated CaBP1 EF hand mutants (grey), CaBP1 (orange), or CaM (blue). **B**, t_{i300} values for data from '**A**'. **C,** Relative current amplitude changes of I_{Ca} in response to 40 +20 mV pulses delivered at 3 Hz for $Ca_V1.2$ expressed with $Ca_V\beta_{2a}$ and the indicated chimeras indicated CaBP1 EF hand mutants, CaBP1, or CaM. **D,** Averaged frequency dependent change of I_{Ca} current amplitude for $Ca_V1.2$ expressed with $Ca_V\beta_{2a}$ and the indicated chimeras indicated CaBP1 EF hand mutants, CaBP1, or CaM. Parentheses indicate the number of oocytes tested. Error bars indicate s.d. P-values with respect to wild-type were calculated using student's t-Test: N.S., not significant, $P > 0.05$; ***, $P < 0.005$.

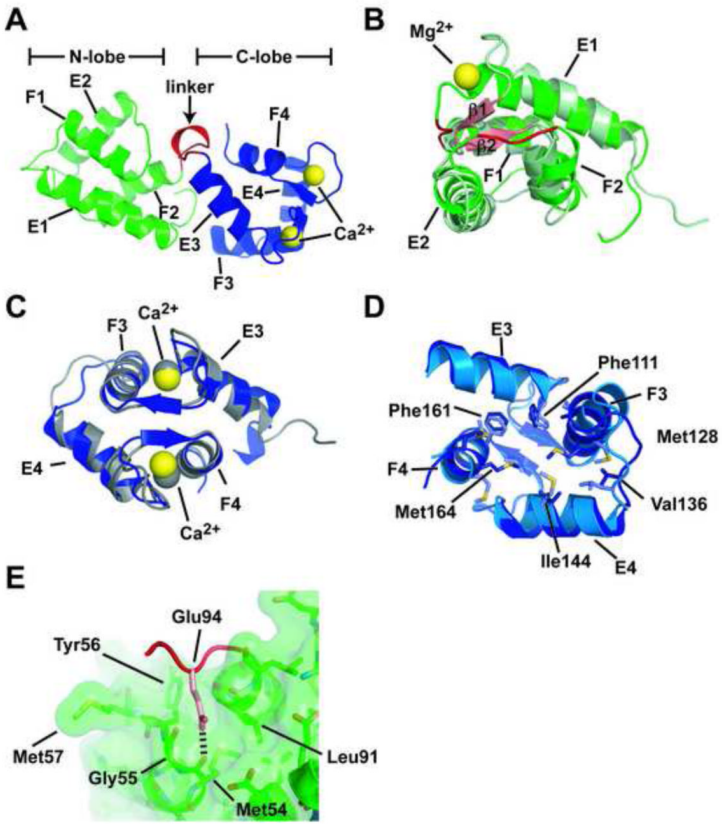

Figure 5.

Structure of CaBP1. **A**, Cartoon representation of CaBP1. N-lobe (green), linker (red), and C-lobe (blue) are indicated. Calcium ions are depicted as yellow spheres. Secondary structure elements are labeled. **B**, Superposition of CaBP1 apo-N-lobe structure determined by X-ray (green) and Mg^{2+}-bound form determined by NMR (2K7B)(Li et al., 2009) (light green). Mg^{2+} ion is a yellow sphere. B-hairpin from the Mg^{2+}-bound form is shown (salmon) and labeled. Equivalent residues in the apo-lobe structure are highlighted in red. **C,** Superposition of CaBP1 Ca^{2+}/C-lobe structure determined by X-ray (blue) and NMR (grey). **D**, Superposition of CaBP1 Ca^{2+}/C-lobe (dark blue) and CaM Ca^{2+}/C-lobe (marine) (1EXR) (Van Petegem et al., 2005). Hydrophobic residues involved in CaM Ca^{2+}/C-lobe-IQ domain binding and their CaBP1 Ca^{2+}/C-lobe counterparts are shown as sticks. **E,** Details of the Glu94/N-lobe cleft interaction. Glu94 and residues from the N-lobe are shown as sticks. N-lobe is colored green and shown in surface representation. Linker is indicated in red. E94 is shown in salmon. Hydrogen bond interaction between E94 and the backbone carbonyls of Met54 is shown as black dashes. See also Figure S3.

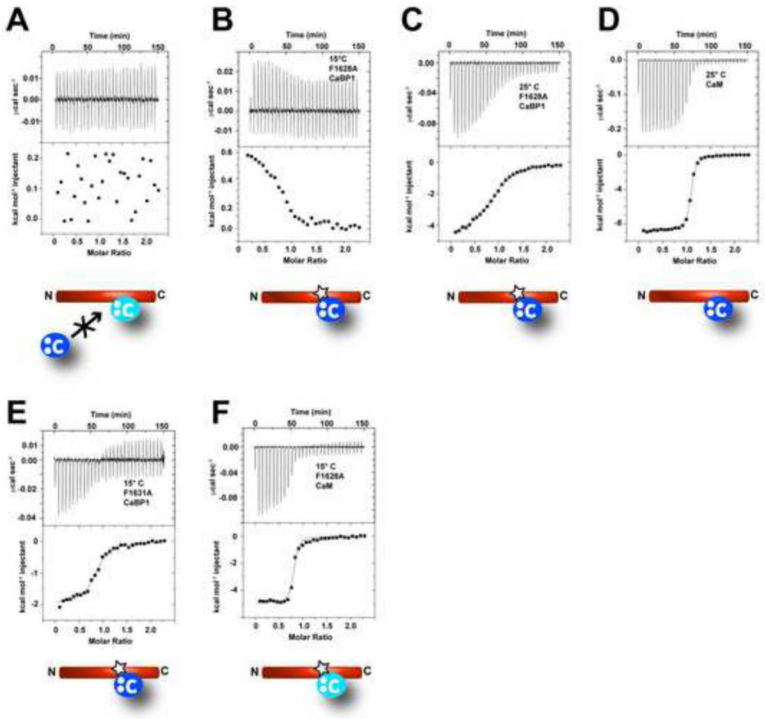

Figure 6.

Ca^{2+}/C-lobe$_{BP}$ and Ca^{2+}/C-lobe$_{CaM}$ binding sites overlap on the $Ca_V1.2$ IQ domain. Exemplar ITC titrations for: **A,** 75 μM Ca^{2+}/C-lobe$_{BP}$ into a solution of 7.5 μM IQ domain and 11.25 μM Ca^{2+}/C-lobe$_{CaM}$. **B,** 75 μM Ca^{2+}/C-lobe$_{BP}$ into 7.5 μM IQ domain F1628A mutant, 15°C. **C**, 75 μM Ca^{2+}/C-lobe$_{BP}$ into 7.5 μM IQ domain F1628A mutant, 25°C. **D**, 75 μM Ca^{2+}/C-lobe$_{BP}$ into wild-type IQ domain, 25°C. **E,** 75 μM Ca^{2+}/C-lobe$_{BP}$ into 7.5 μM IQ domain F1631A mutant. **F,** 75 μM Ca^{2+}/C-lobe$_{CaM}$ into 7.5 μM IQ domain F1631A mutant. Cartoons depict the observed binding modes for Ca^{2+}/C-lobe$_{BP}$ (dark blue) and Ca^{2+}/C-lobe$_{CaM}$ (light blue). Stars indicate mutant IQ domains.

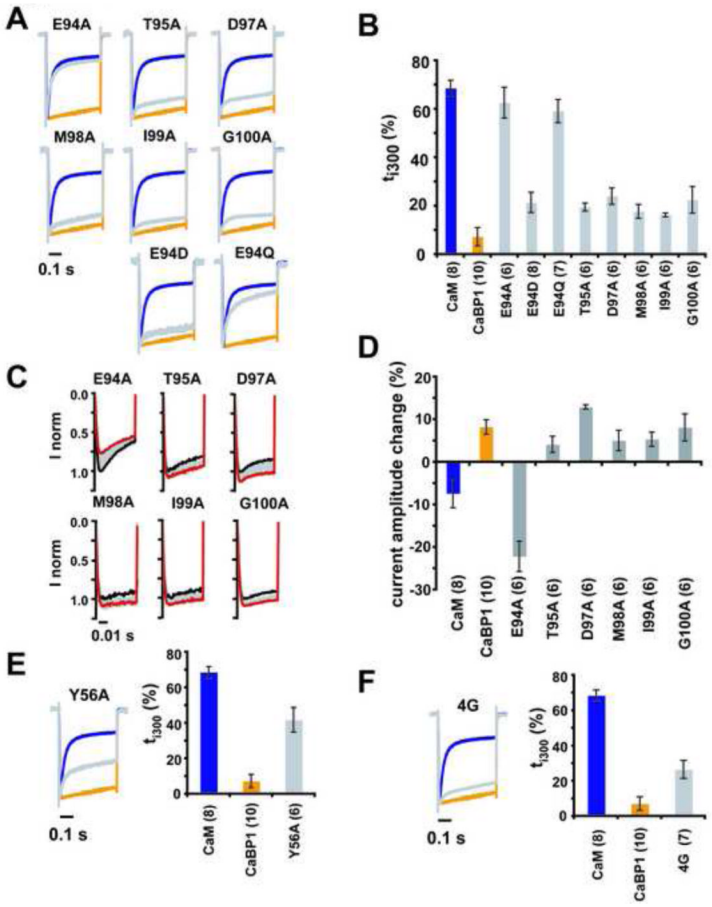

Figure 7.

Functional examination of the CaBP1 interlobe linker and E94/N-lobe interaction. **A**, Representative normalized I_{Ca} traces at a test potential of +20 mV for $Ca_V1.2$ expressed with $Ca_V\beta_{2a}$ and indicated CaBP1 linker mutants (grey), CaBP1 (orange), or CaM (blue). **B**, t_{i300} values for data from '**A**'. **C,** Relative current changes between the last and first pulse for $Ca_V1.2$ expressed with $Ca_V\beta_{2a}$ and CaBP1, CaM, or the indicated mutants. **D,** Averaged frequency dependent change of I_{Ca} amplitude for '**C**'. **E**, and **F,** Representative normalized I_{Ca} traces at a test potential of +20 mV for $Ca_V1.2$ expressed with $Ca_V\beta_{2a}$ and indicated CaBP1 mutants (grey), CaBP1 (orange), or CaM (blue). Graphs compare t_{i300} values. Parentheses indicate the number of oocytes tested. Error bars indicate s.d. See also Figure S4 and Figure S6.

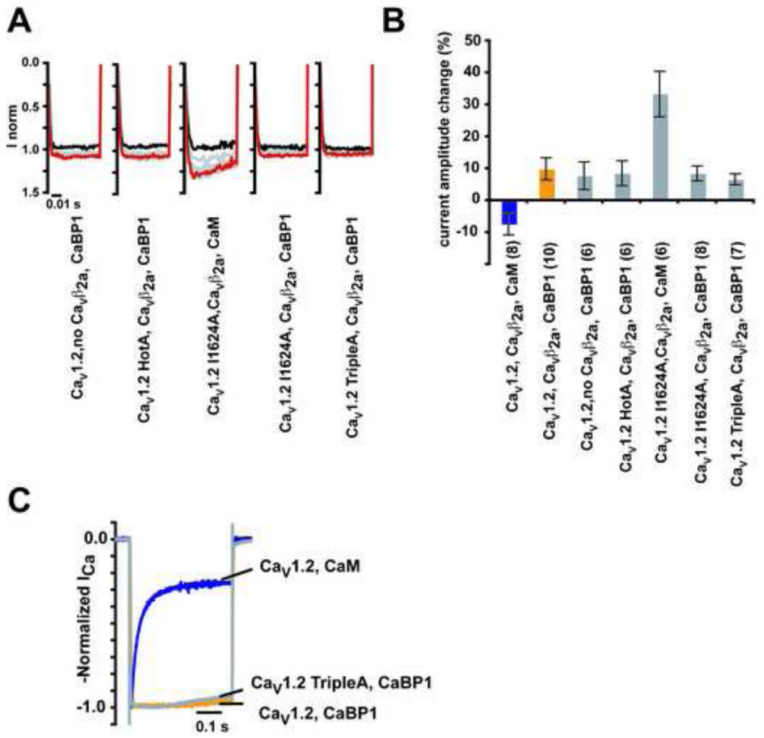

Figure 8.

Comparison of CaBP1-mediated and CaM-mediated $Ca_V1.2$ CDF. **A**, Relative current changes between the last and first pulse in response to 40 +20 mV pulses delivered at 3 Hz for $Ca_V1.2$ and $Ca_V1.2$ mutants expressed with indicated $Ca_V\beta_{2a}$, CaBP1, and CaM combinations. **B,** Averaged frequency dependent change of I_{Ca} amplitude for '**A**'. **C**, Representative normalized I_{Ca} traces at a test potential of +20 mV for $Ca_V1.2$ with $Ca_V\beta_{2a}$ and CaBP1 (orange) or CaM (blue) and $Ca_V1.2$ TripleA (grey) expressed with $Ca_V\beta_{2a}$ and CaBP1. Parentheses indicate the number of oocytes tested. Error bars indicate s.d.

Table 1

$Ca_V1.2$ inactivation parameters

		t_{300} (%)	A_1 (%)	τ_1 (ms^{-1})	A_2 (%)	τ_2 (ms^{-1})	CDF_{40}	N
CaM		68.7 ± 3.2	54.8 ± 5.3	26.2 ± 4.0	17.5 ± 4.4	131 ± 30	- 7.4 ± 3.4	8
CaBP1		7.4 ± 3.8	-	-	-	-	8.8 ± 3.1	10
CaBP1 G2A		9.3 ± 5.3	-	-	-	-	6.8 ± 6.4	6
CaBP1 Δ2-15		6.3 ± 3.1	-	-	-	-	3.1 ± 3.8	6
CaBP1-CaM Chimeras	MMB	70.6 ± 5.1	56.1 ± 4.6	25.1 ± 2.8	18.8 ± 2.6	135 ± 28	- 6.7 ± 1.0	6
	MBM	63.8 ± 5.1	49.0 ± 3.6	26.8 ± 2.6	18.7 ± 4.5	126 ± 13	- 7.0 ± 0.9	6
	MBB	68.6 ± 4.1	55.6 ± 2.1	25.5 ± 2.1	16.8 ± 3.4	131 ± 17	- 8.4 ± 1.7	6
	BMM	33.0 ± 13.3	41.6 ± 12.0	187 ± 41	-	-	- 6.0 ± 1.7	9
	BBM	0.3 ± 0.5	-	-	-	-	22.4 ± 6.2	7
	BMB	63.7 ± 11.8	43.8 ± 8.4	25.5 ± 2.2	26.8 ± 3.8	177 ± 42	-18.6 ± 3.5	6
EF hand mutants	CaBP1 EF1	11.0 ± 5.2	-	-	-	-	11.7 ± 8.4	6
	CaBP1 EF3	23.2 ± 3.8	26.6 ± 6.3	152 ± 49	-	-	- 3.4 ± 4.4	7
	CaBP1 EF4	17.0 ± 5.9	21.0 ± 7.6	171 ± 56	-	-	3.6 ± 3.3	9
	CaBP1 EF34	17.8 ± 6.3	23.7 ± 4.9	181 ± 70	-	-	- 0.4 ± 1.3	7
	CaBP1 AETA	70.0 ± 2.1	54.1 ± 2.6	29.2 ± 1.4	20.7 ± 1.3	171 ± 22	- 34.4 ± 9.2	6
	CaBP1 DMIG	69.6 ± 6.5	51.3 ± 4.6	25.6 ± 3.2	25.5 ± 5.6	193 ± 45	- 27.6 ± 4.5	10
	CaBP1 DTDSDTDS	61.7 ± 10.9	46.8 ± 8.2	24.2 ± 3.1	22.3 ± 5.8	203 ± 68	- 23.4 ± 4.1	6
Interlobe linker mutants	CaBP1 4G	26.8 ± 5.1	25.4 ± 4.4	90.7 ± 44.7	-	-	3.2 ± 4.4	7
	CaBP1 8G	64.4 ± 6.2	51.1 ± 5.6	22.9 ± 2.5	18.6 ± 0.7	162 ± 17	- 27.5 ± 3.0	6
	CaBP1 8A	71.6 ± 5.4	53.2 ± 4.5	21.5 ± 0.7	23.0 ± 3.6	131 ± 13	-16.4 ± 2.2	6
	CaBP1 E94A	62.7 ± 6.4	47.9 ± 5.1	25.0 ± 2.8	21.0 ± 2.5	183 ± 33	- 22.1 ± 3.6	6
	CaBP1 E94Q	59.2 ± 4.9	40.9 ± 4.6	26.0 ± 3.8	26.1 ± 5.2	213 ± 32	-16.9 ± 3.0	7
	CaBP1 E94D	20.2 ± 2.8	19.7 ± 5.2	133 ± 69	-	-	8.6 ± 5.9	8
	CaBP1 T95A	24.5 ± 6.2	23.3 ± 6.6	88.9 ± 23.5	-	-	6.6 ± 3.8	6
	CaBP1 D97A	22.6 ± 4.1	19.7 ± 5.5	121 ± 56	-	-	14.4 ± 2.3	6
	CaBP1 M98A	17.8 ± 2.9	15.0 ± 2.9	64.0 ± 11.2	-	-	5.1 ± 2.4	6
	CaBP1 I99A	18.0 ± 2.9	18.1 ± 2.7	103 ± 23	-	-	6.2 ± 2.9	6
	CaBP1 G100A	22.6 ± 5.5	21.6 ± 5.8	41.5 ± 9.8	-	-	8.2 ± 3.2	6
CaBP1 Y56A		41.9 ± 6.9	30.6 ± 4.6	24.9 ± 1.1	20.3 ± 4.8	280 ± 96	- 0.2 ± 5.5	6
CaBP1 K130A		7.2 ± 5.3	-	-	-	-	6.8 ± 4.2	6
$Ca_V1.2$ TripleA, $Ca_V\beta_{2a}$, CaBP1		3.9 ± 3.0	-	-	-	-	6.7 ± 1.7	7
$Ca_V1.2$ HotA, $Ca_V\beta_{2a}$, CaBP1		23.6 ± 8.4	29.1 ± 8.2	171 ± 65	-	-	11.9 ± 4.0	6
$Ca_V1.2$, no $Ca_V\beta$, CaBP1		13.6 ± 6.3	22.3 ± 2.6	191 ± 22	-	-	10.9 ± 4.1	6
$Ca_V1.2$ I1624A, $Ca_V\beta_{2a}$, CaM		17.5 ± 11.3	18.1 ± 12.1	88.9 ± 9.7	-	-	33.8 ± 10.8	6
$Ca_V1.2$ I1624A, $Ca_V\beta_{2a}$, CaBP1		5.3 ± 2.8	-	-	-	-	8.6 ± 2.3	8

Data are expressed as mean values ± standard deviation. All experiments correspond to the mean of at least two separate oocyte batches.

Table 2

Titration calorimetry data

Cell	Syringe	T (°C)	N	K_d (nM)	n	ΔH (kcal mol^{-1})	ΔS (cal mol^{-1} K^{-1})	K_a/K_a (wt)	ΔΔG (kcal mol^{-1})
Cav1.2 IQ	Ca^{2+}/N-lobe$_{BP}$	15	0.82 ± 0.05	1,100 ± 80	3	2.09 ± 0.40	34.5 ± 1.5	-	-
	Ca^{2+}/C-lobe$_{BP}$	15	0.90 ± 0.07	10.5 ± 1.9	4	−2.88 ± 0.19	26.5 ± 0.6	-	-
	Ca^{2+}/C-lobe$_{BP}$	25	0.98 ± 0.11	15.0 ± 0.7	2	−8.63 ± 0.24	6.9 ± 0.9	-	-
	Ca^{2+}/C-lobe$_{CaM}$*	15	0.98 ± 0.18	2.63 ± 0.07	2	−6.77 ± 0.24	15.75 ± 0.78	-	-
Cav1.2 IQ Ca^{2+}/N-lobe	Ca^{2+}/C-lobe$_{BP}$	15	0.96 ± 0.01	16.6 ± 0.7	2	−3.17 ± 0.05	24.1 ± 0.7	-	-
	Ca^{2+}/CaBP1	15	0.93 ± 0.12	0.288 ± 0.070	2	−4.72 ± 0.07	26.6 ± 0.7	-	-
	Ca^{2+}/CaBP1 E94A	15	1.04 ± 0.04	0.336 ± 0.097	2	−7.75 ± 0.31	15.9 ± 0.5	0.86 ± 0.32	−0.06 ± 0.22
Cav1.2 IQ F1628A	Ca^{2+}/C-lobe$_{BP}$	25	0.88 ± 0.03	727 ± 224	2	−4.87 ± 0.11	11.8 ± 1.0	0.021 ± 0.006	−2.25 ± 0.18
CaV1.2 IQ F1631A	Ca^{2+}/C-lobe$_{BP}$	15	0.83 ± 0.03	345 ± 107	2	−2.22 ± 0.20	21.9 ± 1.3	0.030 ± 0.011	−1.82 ± 0.21
	Ca^{2+}/C-lobe$_{CaM}$	15	0.80 ± 0.03	17.3 ± 4.3	2	−4.87 ± 0.08	18.7 ± 0.8	0.152 ± 0.038	−1.22 ± 0.14

Data are expressed as mean values ± standard deviation. ΔΔG is calculated with respect to the wild-type lobe or protein at 15°C with the exception of data for F1628A, which are calculated at 25°C.

* indicates values from (Van Petegem et al., 2005). See also Figure S5.

Table 3

Crystallographic data collection and refinement statistics

	CaBP1	**CaBP1 K130A**			
Data Collection		Native	SeMet		
Space group	I23	$P3_121$	$P3_121$		
Cell dimensions a/b/c (Å)	206, 206, 206	69, 69, 344	69, 69, 345		
α/β/γ (°)	90, 90, 90	90, 90, 120	90, 90, 120		
Resolution (Å)	50-2.9 (3.06 – 2.90)	50 - 2.4 (2.53 - 2.40)	50-2.9 (3.06 - 2.90)		
			Peak	Inflection	Remote
Wavelength	1.11587	1.11587	0.97958	0.97972	1.01987
Rsym (%)	9.5 (45.1)	7.2 (43.2)	9.0 (38.2)	8.5 (34.9)	7.9 (28.6)
I / σI	6.4 (1.6)	7.1 (1.6)	6.7 (1.8)	6.9 (2.0)	7.2 (2.4)
Completeness (%)	97.5 (96.2)	99.4 (99.0)	100.0 (100.0)	100.0 (100.0)	99.9 (100.0)
Redundancy	4.0 (2.1)	3.9 (2.8)	6.9 (7.2)	6.9 (7.2)	6.9 (7.2)
Unique reflections	32321	43362			
Average B-factor	99.7	54.4			
Refinement					
R_{work}/R_{free} (%)	21.3 / 25.0	25.2 / 29.5			
No. of chains in AU	6	6			
No. of protein atoms	7093	6835			
No. of ligand atoms	12	42			
RMSD bond lengths (Å)	0.020	0.016			
RMSD angles (°)	1.697	1.556			
Ramachandran best /disallowed regions (%)	94.9/0.0	96.1/0.0			

One crystal was used for each dataset. Values in parentheses are for highest-resolution shell.